Molecular Dynamics with Helical Periodic Boundary Conditions

Jiří Kessler[a,b] and Petr Bouř*[a]

Helical symmetry is often encountered in nature and thus also in molecular dynamics (MD) simulations. In many cases, an approximation based on infinite helical periodicity can save a significant amount of computer time. However, standard simulations with the usual periodic boundary conditions (PBC) are not easily compatible with it. In the present study, we propose and investigate an algorithm comprising infinitely propagated helicity, which is compatible with commonly used MD software. The helical twist is introduced as a parametric geometry constraint, and the translational PBC are modified to allow for the helical symmetry via a transitional solvent volume. The algorithm including a parallel code was implemented within the Tinker software. The viability of the helical periodic boundary conditions (HPBC) was verified in test simulations including α-helical and polyproline II like peptide structures. For an insulin-based model, the HPBC dynamics made it possible to simulate a fibrillar structure, otherwise not stable within PBC.

DOI: 10.1002/jcc.23653

Introduction

Being a commonplace in living systems, helical symmetry is often encountered also in their molecular dynamics (MD) simulations. Typical objects involve not only simple helical biopolymers (peptide helices, nucleic acids), but also larger and complex molecular assemblies, such as multithread muscle filaments,[1] amyloid-β fibrils forming Alzheimer's plaques,[2] or tubular networks supporting the cytoskeleton.[3]

Possible ways of tackling such nonperiodic systems include extensive solvation shells,[4] active site solvation,[5] or a hybrid explicit/implicit solvation model.[6] The shell models, such as the primary hydration shell method,[7] are often used when the standard periodic boundary conditions (PBC) are computationally very demanding. The translational periodicity is often desirable, for example, when the lattice–sum interactions are used and the periodicity elegantly increases the effective solvent volume seen by the molecule under investigation. It is compatible with parallelization of the computer code for short-range potentials,[8] for example, using distributions on graphical cards,[9] or potentially makes it amenable to analytical Ewald-like or other pairwise electrostatic summation techniques.[10]

As we are not aware of any MD software directly allowing for the helical periodicity, we investigate here a new algorithm suited to both infinite covalent systems and periodic molecular complexes. It is compatible with commonly used MD procedures and force fields. We implemented and tested it within the Tinker MD package[11] and Amber99[12] force field. The helicity is introduced for a part of the simulated system, which requires minor adjustments of the MD propagation algorithm only.

In this article, we define the helical periodic conditions, discuss the necessary modification of the propagation algorithm, and details of the implementation. For the example of α- and polyproline II helices, we compare the results with the usual PBC computations not using the helical symmetry. As the most applied example, simulation of a fibrillar system based on the insulin molecule is presented. The possibility to determine the overall twist on the run during the MD propagation is discussed as a possible future extension of the method. The results show that the algorithm is stable within a reasonable range of parameters and appears universally applicable as documented on the model systems.

The Helical Periodic Boundary Conditions (HPBC)

Within the standard rectangular PBC, the elementary cell is replicated by a translation. For an atom with a position vector **r,** the replicated positions are $\mathbf{r}' = \mathbf{a} + \mathbf{r}$, where the translational vector **a** is obtained by integer multiplications of the box dimensions b_x, b_y, b_z, ($a_\alpha = n_\alpha \times b_\alpha$, $n_\alpha = 0, 1, 2, \ldots$). Within HPBC, the helical periodicity (say in direction z) is introduced for a central part of the box, within a cylinder of radius r_1 (Fig. 1). This part would typically contain the molecule of interest and part of the solvent environment. During the replication, the cylinder is translated, that is, shifted by b_z, and rotated about its (helical) axis, by an angle φ_0. The rotation is symbolized by the matrix $\mathbf{U}(\varphi_0)$; the replicated positions can be

[a] Jiří Kessler, Petr Bouř
Institute of Organic Chemistry and Biochemistry, Academy of Sciences, Flemingovo náměstí 2, 166 10, Prague, Czech Republic
E-mail: bour@uochb.cas.cz
[b] Jiří Kessler
Department of Physical and Macromolecular Chemistry, Faculty of Science, Charles University, Hlavova 8, 128 40, Prague, Czech Republic
Contract grant sponsor: Academy of Sciences; Contract grant number: M200551205; Contract grant sponsor: Grant Agency of the Czech Republic; Contract grant number: P208/11/0105; Contract grant sponsor: Ministry of Education; Contract grant number: LH11033 and LM2010005

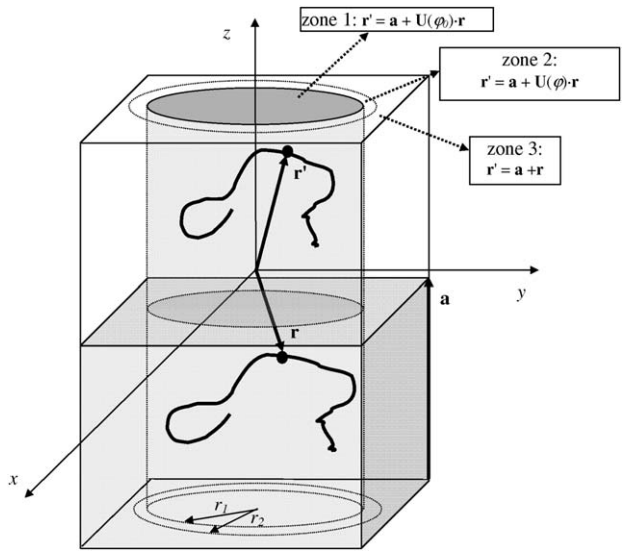

Figure 1. The helical periodic boundary conditions: within the inner cylinder (zone 1) molecules are translated and rotated by the angle φ_0; In the transition zone 2, a partial rotation by $\varphi = f\ \varphi_0$ is applied, and in zone 3 vertical translation by **a** takes place. **U** is the rotational matrix, **r** and **r'** are vectors pointing to an identical atom in neighboring boxes, *f* is a damping function, $f = 1$ and $f = 0$ at the walls of the inner and outer cylinder, respectively, see Figure 2.

expressed as $\mathbf{r}' = \mathbf{a} + \mathbf{U}(\varphi_0) \cdot \mathbf{r}$. As this is incompatible with PBC, a transition zone is defined by an annular space between the above mentioned cylinder (radius r_1) and another cylinder of radius r_2. Within the zone, an intermediate transformation takes place, as defined by $\mathbf{U}(\varphi)$, where $\varphi = f\ \varphi_0$, and *f* is a transition function.

The transition function "damps' the helicity, that is, $f = 1$ and 0 at the wall of the inner and outer cylinder, respectively. Similarly as other potential-adjusting functions, for example, van der Waals or Coulomb interaction cutoffs[4,13] it is desirable that *f* is simple, smooth, and perturbs this system as little as possible, which restricts its choice to a sigmoidal dependence. We chose

$$f(p) = \frac{1}{2}\left(1-(2p-1)\sqrt{\frac{d+1}{d+(2p-1)^2}}\right)$$

where $p = (r_{xy} - r_1)/(r_2 - r_1)$, r_{xy} being the distance from the *z*-axis, and the steepness parameter $d = 0.1$ (Fig. 2, left). Trial computations indicated that the model is not too sensitive to variation of the *d* parameter, although extreme values may lead to dynamic instabilities.

The introduction of the transition zone has little effect on the properties of the periodic simulated system if it is sufficiently separated from the central part of interest (see below). However, it introduces transition regions at the bottom and top of the cylinder, which may lead to serious instabilities during the MD simulation. The source of the problem is depicted at the right hand side of Figure 2, where we display a replication of two atoms (*a* and *b*) within the transitional zone along the helical axis. After a rotation and translation to the neighboring cell the interatomic distance r_{ab} may change, because the atoms *a* and *b* may not be rotated by the same angle. Note that this "deformation" does not affect the actual geometry within the box but only the "virtual" replicas used in the interaction with the environment. Only a small fraction of atoms close to the walls parallel with the *xy* plane and close to zone 2 is affected. Still, if untreated, the rotation causes instabilities in the annular regions close to the wall (*xy* plane) of the box. Most seriously, a solvent molecule passing through the wall may suddenly change its geometry, or a replicated atomic image may move much faster than the atom in the original box.

Fortunately, the problems can be overcome by modification of the propagation algorithm. Complete solvent molecules were rotated while producing the replicas, as based on the

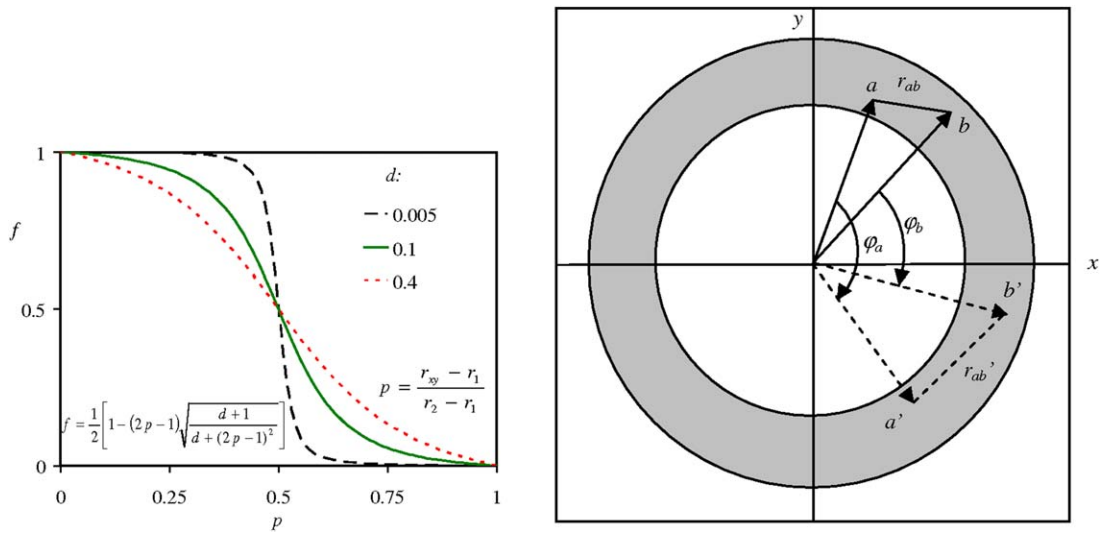

Figure 2. Examples of the damping function (left) and the deformation problem in the transition zone (right): after a rotation and translation about the helical axis (*z*, being perpendicular to the diagram) the distance r_{ab} between two atoms (*a* and *b*, prime denoting the rotated system) may not be conserved, as the rotation angles generally differ, $\varphi_a \neq \varphi_b$. See text for further explanation.

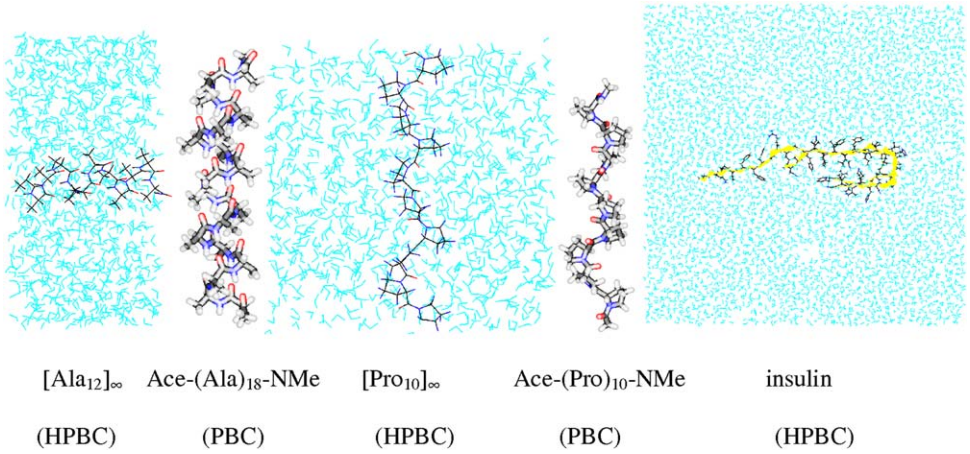

Figure 3. The model systems: HPBC simulation of polyalanine α-helix ($[Ala_{12}]_\infty$), Ace-$(Ala)_{18}$-NMe α-helix with PBC, HPBC simulation of polyproline II polyproline ($[Pro_{10}]_\infty$), the Ace-$(Pro)_{10}$-NMe peptide simulated with PBC, and insulin HPBC simulation. Water is not displayed in the PBC cases, and the plots are not to scale.

damping function determined for their mass centers. This prevented deformations of the geometry of individual molecules. Additionally, passing of molecules through the wall along the helical axis (*z* in Fig. 1) within the transitional zone was prevented during MD runs. This was achieved by applying a half-harmonic potential (*V*) for any molecule outside the box, which left it through zone 2, $V = k \times d^{[2]}$, where *d* is the distance from the box *xy* wall, and the force constant *k* was chosen to be 1 kcal/Å$^{[2]}$ ($V = 0$ inside the box). Values of *k* within 1–10 kcal/Å$^{[2]}$ yielded very similar results and did not significantly influence the geometry of interest in simulations not involving transport processes. Finally, for every dynamic integration step, each coordinate increment (Δr_a) was compared to a corresponding increment in the neighboring replicated box ($\Delta r_a'$). In cases when the latter shift was considerably larger ($|\Delta r_a'| > 1.1|\Delta r_a|$) the former shift was scaled down by a factor of $\Delta r_a/\Delta r_a'$.

Implementation

The HPBC were implemented within the Tinker[11] program. Full parallelization of the code was achieved under the OMP environment (see http://openmp.org/, a link to the adapted Tinker program can be found at http://hanicka.uochb.cas.cz/~bour/programs/list.html). The Amber99[12] force field (comprising the TIP3P[14] force field for water) was used without bond length constraints. The helical periodicity was applied to all the energy and gradient terms, that is, those associated with bond lengths, bond and torsional angles, improper torsions, van der Waals (Lennard–Jones), and point charge electrostatic interactions. All simulations were performed in *NVT* conditions and default Tinker parameters, using the default 9 Å cutoff distance both for van der Waals and Coulomb interactions. The cutoff was combined with potential switching and shifting,[15] using fifth-degree multiplicative and seventh-degree additive (Coulomb only) switching functions as implemented in the Tinker program[11] version 6.2. The Beeman[16] propagation scheme, 1 fs integration time step, temperature of 298 K, and the Berendsen[17] thermostat with the coupling parameter of 0.01 ps were used.

Examined Systems

The geometries of the principal studied systems are shown in Figure 3. As the first test system referred here to as $[Ala_{12}]_\infty$, we used an infinite polyalanine chain in α-helical conformation. To allow for a realistic motion and fluctuations of the peptide, 12 alanine residues and 813 water molecules were kept in the 37.2 × 37.2 × 18.56 Å$^{[3]}$ (helical axis) box, using $r_1 = 8$ Å and $r_2 = 17$ Å. Initial peptide backbone torsion angles ($\varphi = -60^\circ$, $\psi = -45^\circ$, and $\omega = 180^\circ$) corresponded to a standard α-helical geometry.[18] After minimization and an equilibrium dynamics, the production run lasted 2 ns.

The twist angles φ_0 for all systems were determined on the basis of canonical values (X-ray data) or standard PBC simulations, and not varied during the dynamics. For ideal α-helix, its ideal value is about 99° per residue[19]; the equilibrium value supported by the Amber99 force field for polyalanine is only slightly larger (100.4° per residue), that is, 126° for $[Ala_{12}]_\infty$. To determine the effect of φ_0 variation on the dynamics, its magnitude for $[Ala_{12}]_\infty$ was additionally varied within 110°–140°. However, we emphasize that this variation goes beyond the implementation of the HPBC scheme (see above), where the twist is to be considered as a constant, similarly as the box dimensions.

For a comparison, standard PBC computation was set up for the Ace-$(Ala)_{18}$-NMe peptide and 2083 water molecules in a 40 × 40 × 40 Å$^{[3]}$ box, using the same standard initial torsion angles of the peptide backbone. To stabilize the helix, the terminal backbone torsion angles were fixed in three aminoacid residues at each (C— and N—) peptide end. Other MD parameters were the same as for the periodic system.

The second test system $[Pro_{10}]_\infty$ involved the polyproline chain in the polyproline II conformation. The system was created as for the α-helix, that is, 10 proline residues and 856 water molecules per a box dimensioned 30 × 30 × 29.9 Å$^{[3]}$. The twist angle φ_0 was changed within ~100°–120°, and the

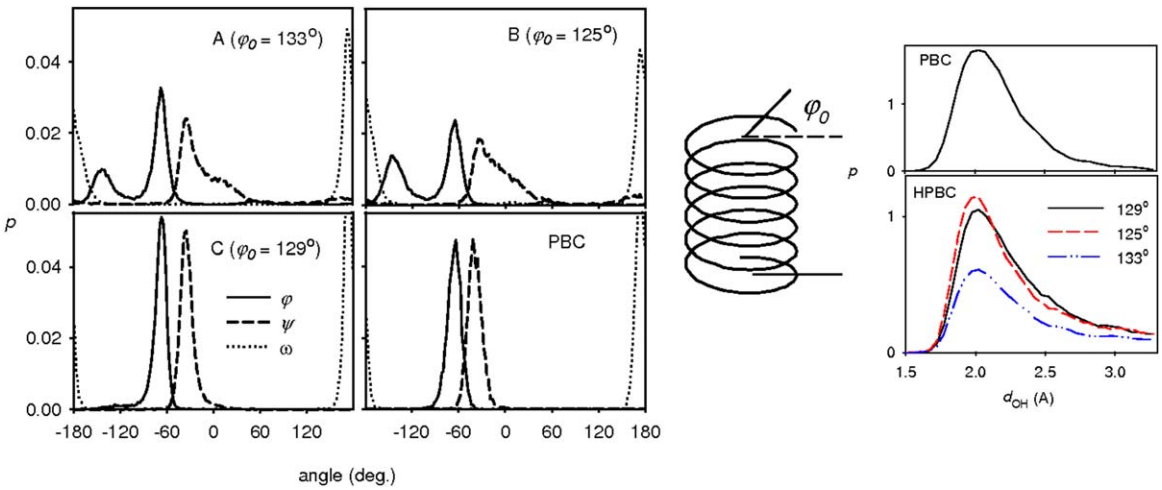

Figure 4. Probability distributions of the peptide main chain angles φ, ψ, and ω (left) and intrahelical hydrogen bond distances (for all NH···O atoms of i, $i+4$ residues, right) in the $[(Ala)_{12}]_\infty$ α-helical polypeptide, as obtained for three twist φ_0 angles, and distributions obtained from the standard PBC simulation. [Color figure can be viewed in the online issue, which is available at wileyonlinelibrary.com.]

initial standard polyproline II peptide backbone torsion angles[18] were set to $\varphi = -75°$, $\psi = 150°$, and $\omega = 180°$. By default, $r_1 = 9$ Å and $r_2 = 13.5$ Å although other dimensions of the transitional zone were also tested as specified below. To estimate a variation along the *z*(helical)-axis, we simulated also shorter ($[Pro_9]_\infty$, 30 × 30 × 26.91 Å$^{[3]}$) and longer ($[Pro_{12}]_\infty$, 30 × 30 × 35.88 Å$^{[3]}{}_\infty$) systems under analogous conditions as for $[Pro_{10}]_\infty$, and compared the results to a reference PBC computation performed for the Ace-$(Pro)_{10}$-NMe peptide and 2097 water molecules in the 40 × 40 × 40 Å$^{[3]}$ box. As for the α-helix, the total time of each simulation was 2 ns.

Finally, the largest system involved protonated insulin molecule (785 atoms), six Cl^- ions, and 4593 water molecules in 110 × 110 × 12 (helical axis) Å$^{[3]}$ box, with $\varphi_0 = 0°$, 3° and 6°, and $r_1 = 43$ Å and $r_2 = 53$ Å. The initial geometry mimicking the likely conformation of insulin in a fibrillar form was based on the β-roll protein (identification code 1VH4 in the protein data bank, http://www.rcsb.org/pdb/). Insulin torsion angles were set to those adopted by residues A256–A306 in the 1VH4 crystal structure.[20] The fibrillation of insulin is a well documented process.[21,22] The system was also partially inspired by the latest spectroscopic experiments using Raman optical activity that provided a new insight into the free insulin structure[23] and fibril formation.[24] On energy minimization and subsequent equilibration the system was let to develop for 300 ps under the default conditions of *NVT* ensemble, 298 K and 1 fs integration step.

For statistical analyses, we used in part our own scripts; resultant probability distributions of angles and distances are normalized ($\int p(x)dx = 1$).

Results and Discussion

Modeling of the α-helix

For the $[Ala_{12}]_\infty$ α-helical model we found a relatively tight dependence of the geometry on the overall twist φ_0. This is documented in Figure 4 where the calculated probability distributions of the peptide main chain torsion angles (φ, ψ, and ω) and the O···HN distances relevant for the intramolecular hydrogen bonds are plotted and compared to those obtained for the standard PBC Ace-$(Ala)_{18}$-NH-Me helical model. All distances measured between amide oxygen and hydrogen atoms of *i*th and $i+4$th aminoacid residues, respectively, were included in the statistics. For $\varphi_0 = 129°$, the average torsion angles ($\varphi = -66°$, $\psi = -35°$, and $\omega = 173°$) and their equilibrium distributions are very close to those obtained by PBC ($\varphi = -64°$, $\psi = -39°$, and $\omega = 173°$). Note that for the PBC model, the helix had to be stabilized by freezing the terminal torsion angles, which are, therefore, not included in the statistics. Nevertheless, both the HPBC and PBC results indicate the Amber99 force field enables standard α-helical polyalanine conformation only when arbitrarily stabilized, that is, by the infinite helicity in the former and by the terminal constraints in the latter simulation.

For the φ_0 twist angles of 133° and 125°, the α-helix is significantly perturbed in the HPBC simulations. The ω-angle is not significantly affected, which corresponds to the relative rigidity of the nearly planar amide group, but the φ and ψ angles are more dispersed, indicating a significant disruption of the regular helical geometry. Similarly, for $\varphi_0 = 129°$, the probability distribution of the hydrogen bond distances reasonably well correspond to the PBC simulation; interestingly, for $\varphi_0 = 133°$ the $i,\ldots,i+4$ hydrogen bonds are much more perturbed than for $\varphi_0 = 125°$.

The HPBC twist also perturbs motion of the solvent molecules. This is difficult to evaluate together with the peptide simulation, where many of the water molecules are hydrogen bonded to the solute. Instead, we applied the helical twist φ_0 to the box of the same size (37.2 × 37.2 × 18.56 Å$^{[3]}$) entirely filled with water. Because we were interested in the translational motion, presumably most affected by the twist, we defined an average translational atomic velocity as $<|r_i(t) - r_i(t-\Delta)|/\Delta>$, with a relatively large integration step of

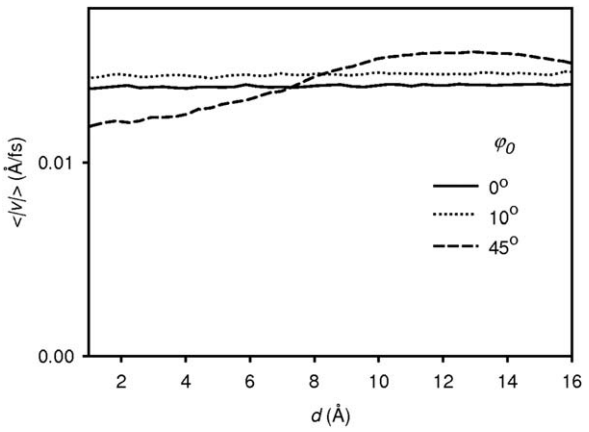

Figure 5. Average translational water atom velocities (see the text for definition) in the 37.2 × 37.2 × 18.56 Å[3] box filled with water only as perturbed by the helical twist, for $r_1 = 8$ Å, $r_2 = 17$ Å, d is the distance from the helical axis.

$\Delta = 10$ fs. Thus the translational motion (and part of the rotational one) could be separated from the vibrational degrees of freedom. The velocity as dependent on the distance from the helical axis is plotted in Figure 5. For φ_0 of 0° and 10°, the velocity is relatively independent of the distance, although for the latter case the solvent already appears to move slightly faster. For the angle of 45°, a larger deformation of the velocity profile appears. For radii approximately smaller than r_1, the velocity decreases, whereas it is larger than in the PBC simulation otherwise. It is, thus, certainly desirable to prefer smaller helical twists, which perturb the solvent motion less.

The HPBC dynamics of $[Pro_{10}]_\infty$

The polyproline II helix, known to well represent the so-called random conformation of general peptides,[25] is more flexible than α-helix. This corresponds to the wider distributions of the φ and ψ torsional angles (Fig. 6). The most probable angles ($\varphi = -69°$ and $\psi \sim 163°$) are almost the same for the HPBC and PBC dynamics. The maximal ω-value of 175° is only somewhat larger than in α-helix (173°) due to the absence of intramolecular hydrogen bonds in the polyproline. Compared to the α-helix, the polyproline structure appears to be more resistant to the overall twist. Nevertheless, for the φ_0 angles of 100° and 105°, the probability distribution already becomes markedly wider than for the most stiff geometry at $\varphi_0 = 110°$. This also corresponds well to the average value of 106.4° estimated from the CH_3CO-$(Pro)_9$-$CONHCH_3$ PBC simulation. The variation of the number of the proline residues ($[Pro_9]_\infty$ vs.

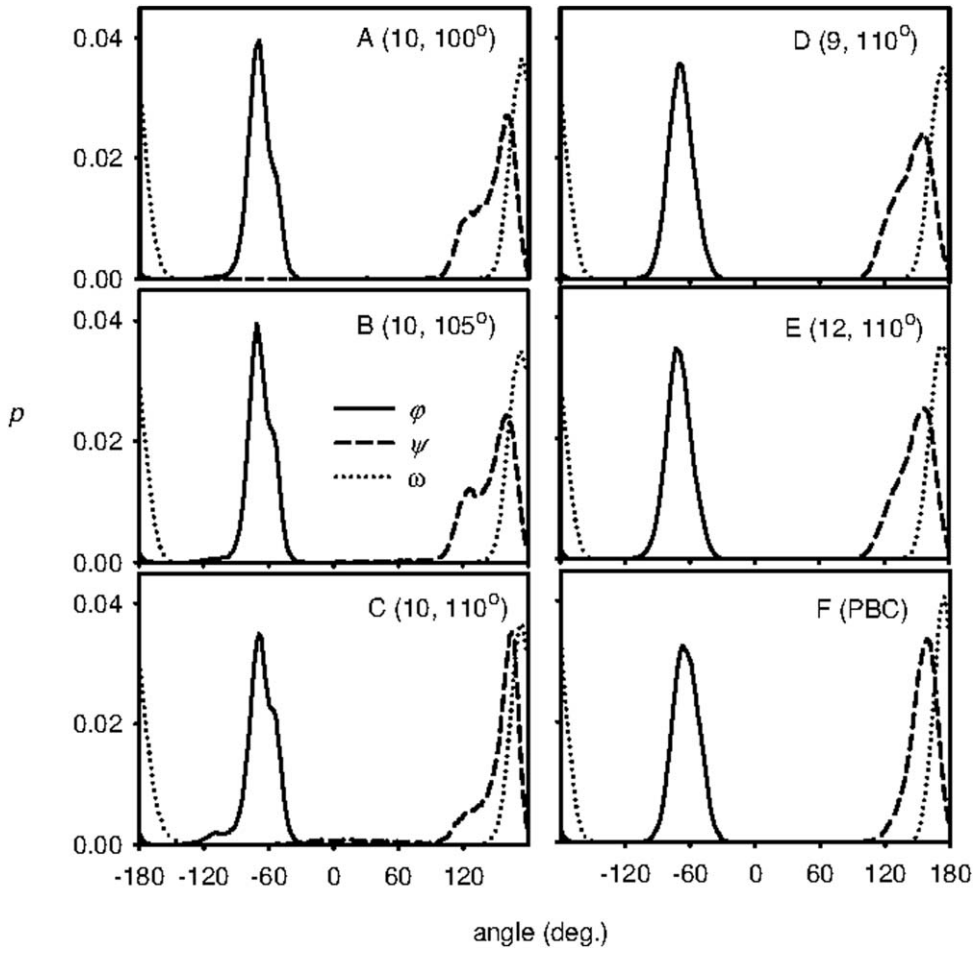

Figure 6. Probability distributions of the main chain torsion angles obtained using HPBC for various $[Pro_N]_\infty$ polyproline II models (panels A–E, the number N of the proline units and the twist φ_0 recalculated to $N = 10$ are indicated) and the PBC simulation of Ac-$(Pro)_9$-NMe (F).

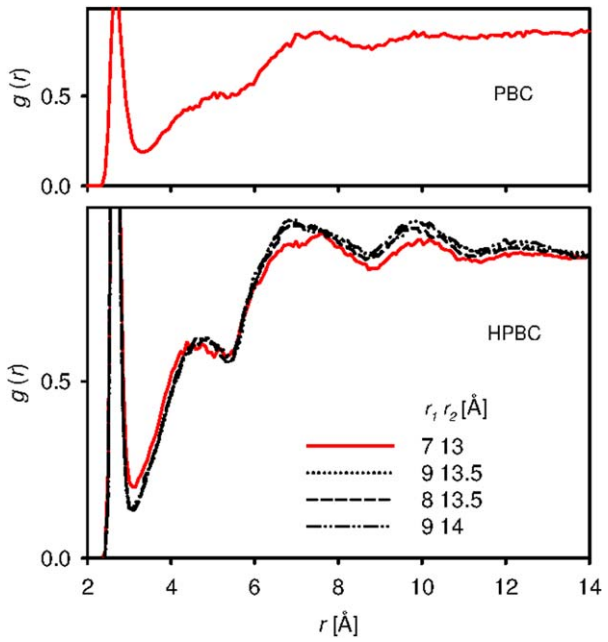

Figure 7. Radial distribution function (amide O···water mass center, bottom) in the $[Pro_{10}]_\infty$ system, as calculated for four different sizes of the transition zone; at the top, radial distribution from the standard PDB simulation of Ace-$(Pro)_{10}$-NMe is plotted. [Color figure can be viewed in the online issue, which is available at wileyonlinelibrary.com.]

$[Pro_{10}]_\infty$ vs. $[Pro_{12}]_\infty$) causes minor changes, mostly affecting the ψ-angle distribution. However, results of $[Pro_9]_\infty$ and $[Pro_{12}]_\infty$ provide a more symmetric distribution of φ than for $[Pro_{10}]_\infty$, due to a fine interplay between the box length and the helical twist.

We are naturally keen to find out if the transitional zone geometry affects the important simulated variables. Therefore, for example, the radial distribution function between an amide oxygen and mass centers of water molecules was calculated as shown in Figure 7 for four sizes of the zone, compared with the standard PBC result. Indeed, as apparent from the figure, if the zone is too close to the polyproline chain ($r_1 = 7$ Å) it perturbs the distribution in a wide range 2–14 Å of the radial distances between amide oxygen and H_2O mass center. For $r_1 = 8$ Å and larger the radial distribution function stabilizes and variations of the transition zone geometry have a negligible influence on it. Note that at the distance of $r_1 = 8$ Å from the helical axis some polyproline atoms are still as close as ~1.5 Å; the effect of the transitional zone on the geometry is thus quite minor and restricted to a short range only. The HPBC radial distribution function well reproduces the main features of the PBC result (Fig. 7, top) calculated for a center amide oxygen in Ace-$(Pro)_{10}$-NMe.

Similarly, for $r_1 = 7$ Å, the distribution of the torsional angles is perturbed in the HPBC dynamics (Fig. 8) but this is readily improved for the radii of 8 Å and greater. For $r_1 = 7$, the distribution of φ becomes wider, and ψ may even adopt a value around $-30°$, very far from the ideal polyproline II structure. Variation of the outer radius r_2 does not seem to have an effect at all, at least with respect to the polyproline geometry and the radial distribution function.

Insulin fibril vs. β-roll geometry

For the insulin model, we want to show that the geometry is compatible with that observed for the β-roll protein, as this would enable a long-range arrangement of the insulin monomeric units in the fibrils. Indeed, owing to the interaction to the box replicas the insulin geometry is quite stable during the HPBC dynamics (Fig. 9), and a fibril similar to the β-roll structure is formed.

The simulation time (300 ps) is rather short; nevertheless the simulations seem to exhibit converged potential energy profiles, and for the zero twist, the average geometry is very close to that obtained by the longer (8 ns) PBC computation (Fig. 10). The largest deviations appear outside the insulin loop for the semifree part of the peptide chain. For PBC, the Amber program[26] enabling a more extensive parallelization than Tinker was used, and the insulin molecule was stabilized by sandwiching it between two other molecules fixed in space in a 110 × 110 × 36 Å[3] box, otherwise the simulation parameters were the same.

In all cases, the conformation required for the fibril formation, thus, appears supported by the Amber99 force field. Additionally, for $\varphi_0 = 0°$ (standard PBCs), the structure is more flexible than for $\varphi_0 = 6°$ (cf. Fig. 9), which, as for the smaller systems' computations documented in Figures 4 and 6, most likely indicates that the latter "twisted" fibrillar geometry is favored by the Amber99 force field, in accord with the experimental observations of the β-roll protein[20] in other fibril studies.[27–30]

We recall that for each system the twist angle φ_0 is treated as a fixed parameter in the MD runs. Still, one can ask, if it can be somehow varied and optimized for each system. This, however, appears difficult. Indirectly, its equilibrium value could be

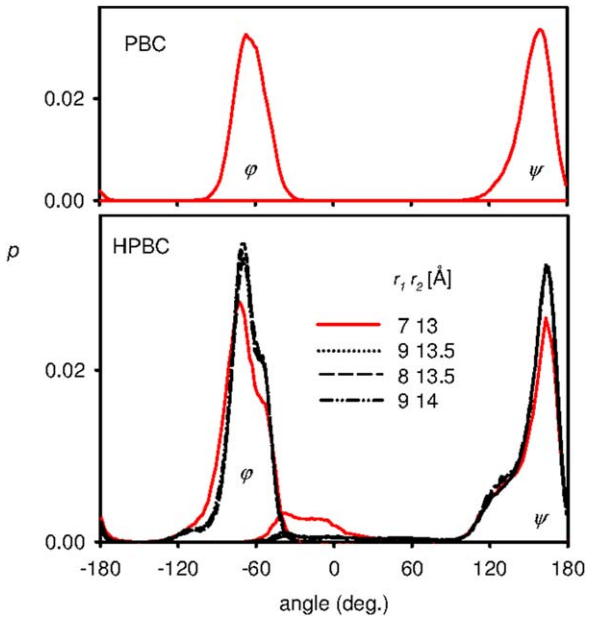

Figure 8. Probabilities of the φ and ψ angles in $[Pro_{10}]_\infty$ calculated for four different sizes of the transitional zone (bottom), and the result for standard PBC (top). [Color figure can be viewed in the online issue, which is available at wileyonlinelibrary.com.]

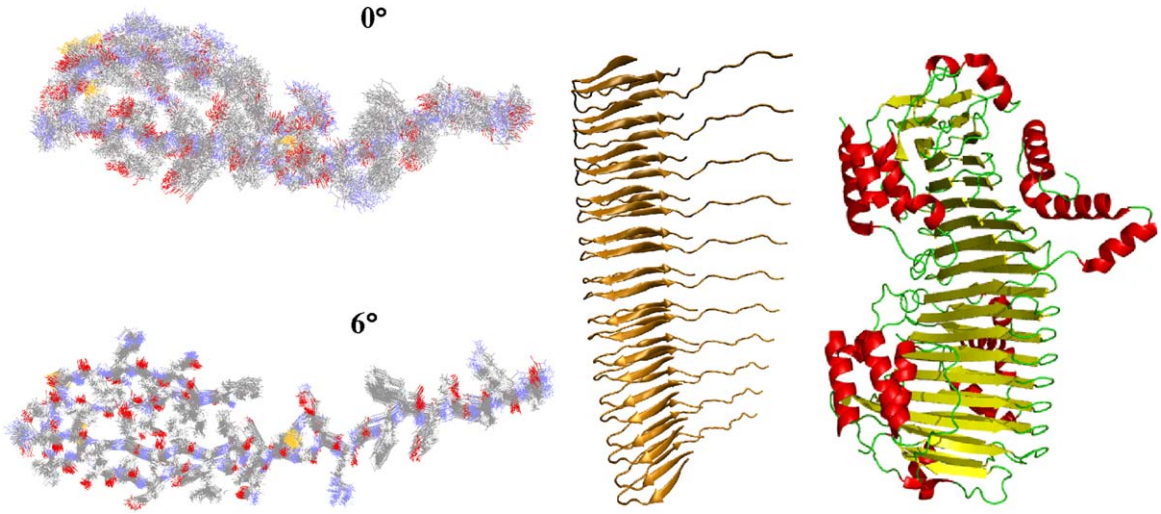

Figure 9. Snapshot overlaps from the HPBC dynamics of the insulin fibril for the twists φ_0 of 0° and 6° (left), the propagated fibril geometry (middle), and the β-roll 1VH4 protein X-ray structure (right). [Color figure can be viewed in the online issue, which is available at wileyonlinelibrary.com.]

estimated from the geometric features of the system, such as those investigated in Figures 4, 6, and 9. We also attempted an alternate evaluation, from the average atomic torque. For each force term (bonds, torsions, bond angles, and pair wise interactions) in each MD step, we calculated the force $\mathbf{f}_i$ acting on an atom i at a position $\mathbf{r}_i$, and the moment $m_{i,z}$ corresponding to the helical axis, $m_{i,z} = f_{i,x}r_{i,y} - f_{i,y}r_{i,x}$. Then, we investigated if the negative moment components $<m_z^->$, averaged over a number of MD steps and atomic contributions, reaches a maximum at an equilibrium value of φ_0. For the $[Pro_{10}]_\infty$ polypeptide in empty and water-filled box, the dependencies of $<m_z^->$ on φ_0 are plotted in Figure 11. The dependence for polyproline in vacuum indicates a relatively sharp maximum for $\varphi_0 \sim 101.5°$. In water, the dependence indicates a maximum at $\varphi_0 \sim 106.0°$, well corresponding to the value of 106.4° from the unconstrained dynamics. Nevertheless, different values of $<m_z^->$ were obtained with independent MD runs for the same φ_0, and the overall precision remained low even for long simulation times, and such method may, thus, not be universally applicable.

Conclusions

We implemented the infinite helicity into the Tinker molecular dynamics program, based on a virtual transitional solvent region in the PBC replicas, where the helical twist angle φ_0 was treated as an additional constant parameter. The transitional region brought about some instabilities into the MD, which, however, could be effectively rectified by additional restraints, and which do not seem to significantly perturb the

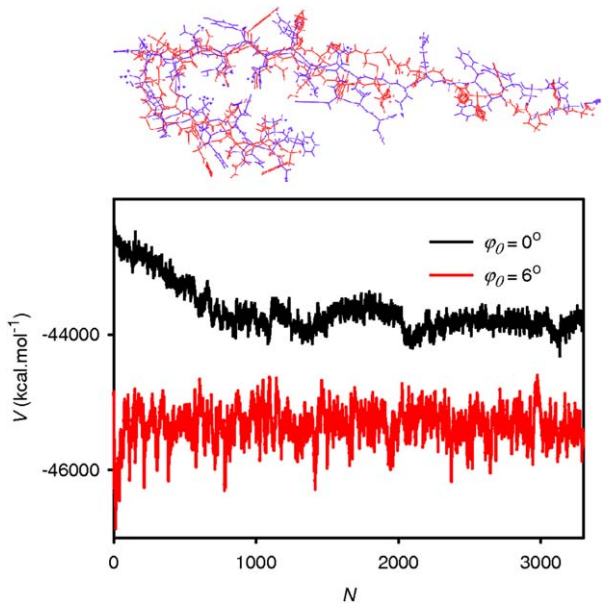

Figure 10. (Top) overlap of the average structures of the insulin fibril model obtained by HPBC (Tinker, $\varphi_0 = 0°$, 0.3 ns) and PBC (Amber99, 8 ns) dynamics, and (bottom) the potential energy from the HPBC simulations for the two twist angles, N is number of the snapshot taken in 100 fs intervals. [Color figure can be viewed in the online issue, which is available at wileyonlinelibrary.com.]

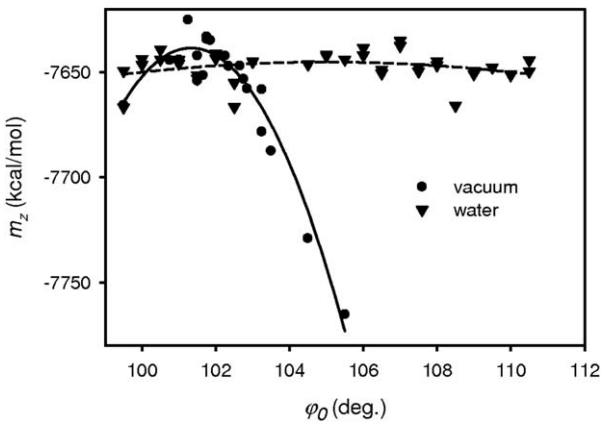

Figure 11. Average m_z torque moment dependent on the twist, as calculated with HPBC for $[Pro_{10}]_\infty$ in vacuum and in the water-filled box. The y-scale for the water was scaled down according to the vacuum values; quadratic fits are indicated by the solid and dashed lines. Note that some MD runs were repeated with different initial velocities, providing different m_z for the same twist angle.

geometry of the studied system. The HPBC dynamics was successfully tested on model systems, appeared to be compatible with common MD algorithms and force fields, and can, thus, be further used in theoretical investigations of the helical structures. For the most complex example, the insulin fibril, the HPBC dynamics made it possible to verify the stability of the fibril-forming conformation, which document the possibilities of this approach for structure and dynamics modeling of larger biologically relevant molecular systems.

Acknowledgments

The authors thank Prof. Shigeki Yamamoto (Osaka University) for the discussion on the insulin structure and Dr. Radek Pelc (Stentor Institute) for helpful comments to the manuscript.

Keywords: periodic boundary conditions · helical symmetry · molecular dynamics · protein structure · amyloid fibrils

How to cite this article: J. ř Kessler, P. Bouř. *J. Comput. Chem.* **2014**, *35*, 1552–1559. DOI: 10.1002/jcc.23653

[1] S. L. Hooper, K. H. Hobbs, J. B. Thuma, *Prog. Neurobiol.* **2008**, *86*, 72.
[2] J. C. Stroud, C. Liu, P. K. Teng, D. Eisenberg, *Proc. Natl. Acad. Sci. USA* **2012**, *109*, 7717.
[3] W. F. Boron, E. L. Boulpaep. Medical Physiology: A Cellular and Molecular Approach; Elsevier/Saunders: Philadelphia, **2003**.
[4] M. P. Allen, D. J. Tildesley. Computer simulation of liquids; Oxford University Press: New York, **1987**.
[5] P. L. Cummins, J. E. Gready, *J. Comput. Chem.* **1996**, *17*, 1598.
[6] G. Brancato, N. Rega, V. Barone, *J. Chem. Phys.* **2008**, *128*, 144501.
[7] M. B. Hamaneh, M. Buck, *J. Comput. Chem.* **2009**, *30*, 2635.
[8] J. Li. In Handbook of Materials Modeling; S. Yip, Ed.; Springer: Amsterdam, **2005**, p 565.
[9] W. Liu, B. Schmidt, G. Voss, W. Müller-Wittig, *Comput. Phys. Commun.* **2008**, *179*, 634.
[10] C. J. Fennell, J. D. Gezelter, J. Chem. *Phys.* **2006**, *124*, 234104.
[11] J. W. Ponder, *Tinker 6.2*, Washington University School of Medicine: Saint Louis, **2000**.
[12] N. Kamiya, Y. S. Watanabe, S. Ono, J. Higo, *Chem. Phys. Lett.* **2005**, *401*, 312.
[13] T. Schlick. Molecular Modeling and Simulation; Springer: Berlin, **2002**.
[14] W. L. Jorgensen, J. Chandrasekhar, J. D. Madura, *J. Chem. Phys.* **1983**, *79*, 926.
[15] P. J. Steibach, B. R. Brooks, *J. Comput. Chem.* **1994**, *15*, 667.
[16] D. Beeman, *J. Comput. Phys.* **1976**, *20*, 130.
[17] H. J. C. Berendsen, J. P. M. Postma, W. F. van Gunsteren, A. Dinola, J. R. Haak, J. *Chem. Phys.* **1984**, *81*, 3684.
[18] T. E. Creighton. Proteins: Structures and Molecular Properties; W. H. Freeman and Co.: New York, **1993**.
[19] S. Kumar, M. Bansal, *Biophys. J.* **1998**, *75*, 1935.
[20] J. Badger, J. M. Sauder, J. M. Adams, S. Antonysamy, K. Bain, M. G. Bergseid, S. G. Buchanan, M. D. Buchanan, Y. Batiyenko, J. A. Christopher, S. Emtage, A. Eroshkina, I. Feil, E. B. Furlong, K. S. Gajiwala, X. Gao, D. He, J. Hendle, A. Huber, K. Hoda, P. Kearins, C. Kissinger, B. Laubert, H. A. Lewis, J. Lin, K. Loomis, D. Lorimer, G. Louie, M. Maletic, C. D. Marsh, I. Miller, J. Molinari, H. J. Muller-Dieckmann, J. M. Newman, B. W. Noland, B. Pagarigan, F. Park, T. S. Peat, K. W. Post, S. Radojicic, A. Ramos, R. Romero, M. E. Rutter, W. E. Sanderson, K. D. Schwinn, J. Tresser, J. Winhoven, T. A. Wright, L. Wu, J. Xu, T. J. R. Harris, *Proteins* **2005**, *60*, 787.
[21] L. Nielsen, S. Frokjaer, J. Brange, V. N. Uversky, A. L. Fink, *Biochemistry* **2001**, *40*, 8397.
[22] J. Brange, L. Anderson, E. D. Laursen, G. Meyn, E. Rasmussen, *J. Pharma. Sci.* **1997**, *86*, 517.
[23] S. Yamamoto, J. Kaminský, P. Bouř, *Anal. Chem.* **2012**, *84*, 2440.
[24] S. Yamamoto, H. Watarai, *Chirality* **2012**, *24*, 97.
[25] R. K. Dukor, T. A. Keiderling, *Biopolymers* **1991**, *31*, 1747.
[26] D. A. Case, I. T. E. Cheatham, T. Darden, H. Gohlke, R. Luo, J. K. M. Merz, A. Onufriev, C. Simmerling, B. Wang, R. Woods, *J. Comput. Chem.* **2005**, *26*, 1668.
[27] H. Chi, W. R. W. Welch, J. Kubelka, T. A. Keiderling, *Biomacromolecules* **2013**, *14*, 3880.
[28] S. Wójcik, V. Babenko, W. Dzwolak, *Langmuir* **2010**, *26*, 18303.
[29] W. Dzwolak, W. Surmacz-Chwedoruk, V. Babenko, *Langmuir* **2013**, *29*, 365.
[30] D. Kurouski, R. K. Dukor, X. Lu, L. A. Nafie, I. K. Lednev, *Chem. Commun.* **2012**, *48*, 2837.

Received: 25 March 2014
Revised: 20 May 2014
Accepted: 26 May 2014
Published online on 10 June 2014